

MIT Open Access Articles

*Global optimization for accurate and efficient
parameter estimation in nanofiltration*

The MIT Faculty has made this article openly available. **Please share**
how this access benefits you. Your story matters.

Citation: Lienhard, John and Rehman, Danyal. 2022. "Global optimization for accurate and efficient parameter estimation in nanofiltration." Journal of Membrane Science Letters, 2 (2).

As Published: 10.1016/j.memlet.2022.100034

Persistent URL: <https://hdl.handle.net/1721.1/145408>

Version: Final published version: final published article, as it appeared in a journal, conference proceedings, or other formally published context

Terms of use: Creative Commons Attribution-NonCommercial-NoDerivs License





Global optimization for accurate and efficient parameter estimation in nanofiltration

Danyal Rehman^{a,b}, John H. Lienhard^{a,*}

^a Rohsenow Kendall Heat Transfer Laboratory, Massachusetts Institute of Technology, Cambridge, MA 02139-4307, USA

^b Center for Computational Science and Engineering, Massachusetts Institute of Technology, Cambridge, MA 02139-4307, USA

ARTICLE INFO

Keywords:

Ion selectivity
Transport models
Metaheuristics
Global optimization
Nanofiltration

ABSTRACT

One of the most well-established frameworks for modeling multicomponent transport in nanofiltration (NF) is the Donnan-Steric Pore Model with Dielectric Exclusion (DSPM-DE). Conventional DSPM-DE characterizes transport across NF membranes through four governing membrane parameters: (1) pore radius; (2) effective membrane thickness; (3) membrane charge density; and (4) the dielectric constant inside the membrane pores. The process for quantifying these parameters is typically sequential. First, neutral solute experiments are performed to determine pore radius and effective membrane thickness. Next, charged species experiments are conducted, and the data is used to regress out the remaining parameters. The resulting regressions are often performed using local search algorithms that can struggle to provide low residuals with robust fits. In addition, this two-step approach tends to: (1) require a substantial number of charged and uncharged solute experiments; and (2) introduce assumed relationships between pore size and water flux, such as the Hagen-Poiseuille equation, which may not be representative of transport through complex pore networks. To address these issues, we propose the use of metaheuristic global optimization techniques supplemented with gradient-free local search and maximum likelihood estimation to simultaneously regress all four membrane parameters directly from charged species experiments. We validate our approach against eight independent datasets across diverse input salinities, compositions, and membranes.

1. Introduction

Membrane-based processes are widely employed for metals recovery, water desalination, and mineral extraction across a diverse range of sourcewaters (Ritt et al., 2022). By avoiding the inefficient recovery of latent heat typical of thermally-driven systems, membrane separations can operate at a substantially lower energy expense, all while maintaining high selectivities (Sholl and Lively, 2016). A relatively well-established method for performing some of these separations is nanofiltration (NF) - a pressure-driven process that exploits steric, dielectric, and Donnan exclusion mechanisms to achieve size- and charge-based separation (Hardian et al., 2022) (see Fig. 1).

NF membranes typically have pore size distributions that lie between ultrafiltration (UF) and reverse osmosis (RO) (Zydney, 2022). Consequently, the steric effects familiar to UF are of commensurate importance to the solution-diffusion mechanisms encountered in RO. The most well-established model for NF that incorporates all of these selectivity mechanisms is commonly referred to as the Donnan-Steric Pore Model with Dielectric Exclusion (DSPM-DE) or the Hindered Electromigration

(HET) Model (Wang and Lin, 2021). We refer to this model as DSPM-DE for the remainder of this work.

In characterizing NF membranes, DSPM-DE is commonly coupled with experiments to enable the quantification of four governing membrane parameters: (1) pore radius, r_p ; (2) effective membrane thickness, Δx_e ; (3) membrane charge density, χ_d ; and (4) the dielectric constant in the membrane pores, ζ_p (Roy et al., 2015). The regression process is a two-step procedure to first quantify r_p and Δx_e through neutral solute experiments, and then to identify χ_d and ζ_p using charged species data.

Using this two-step approach requires a substantial number of experiments, making characterization tedious (Wang et al., 2021). The sequential process is typically justified by the claim that r_p and Δx_e do not change when charged species are introduced; however, whether or not the membranes de-swell in the presence of alternate solutes or varying pH remains unclear and a subject of study (Cheng et al., 2018; Puhan et al., 2022; Shinde et al., 2021; Wang and Lin, 2021). Furthermore, in regressing r_p and Δx_e , an explicit water flux function is required. Most frequently, the Hagen-Poiseuille equation or some variant, is used (Labban et al., 2017; Silva et al., 2005). Furthermore, the

* Corresponding author.

E-mail addresses: drehman@mit.edu (D. Rehman), lienhard@mit.edu (J.H. Lienhard).

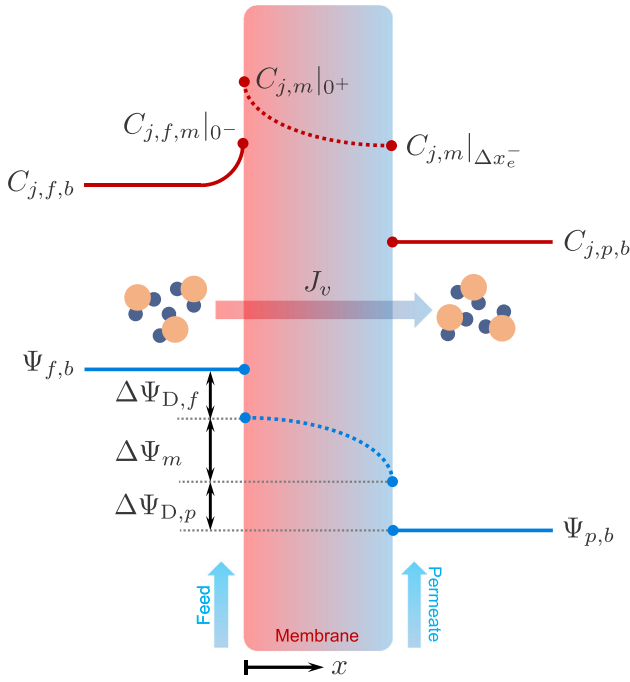


Fig. 1. Transport across the selective layer of an NF membrane with qualitative concentration and electric potential profiles. Diffusion, convection, and cation migration act in the same direction as water flux, while anion migration tends to work in the opposing direction. Subscript j corresponds to species j , while subscripts f and p denote the feed and permeate streams, respectively. In addition, subscripts b and m denote the bulk and membrane, respectively. Positions 0^- and 0^+ denote the fluid-side and membrane-side interface with the feed stream, while position Δx_e^- denotes the membrane-side interface adjacent to the permeate stream. Lastly, C is concentration, J_v is water flux, ψ is electric potential, and $\Delta\psi_D$ in the Donnan potential.

sequential regression strategy can also give rise to regression parameters that deviate from physically-representative values (Kammoun et al., 2020). Wang and Lin also noted that uncertainties in parameter estimation can propagate across experiments: using their mock data, it was noted that a 10% measurement uncertainty in ζ_p could lead to nearly an order of magnitude uncertainty in χ_d (Wang et al., 2021). Consequently, the development of a more reliable and efficient regression framework that alleviates some of these issues could enable a more accurate approach to characterizing NF membranes, with lower data requirements and fewer assumptions.

We propose a new framework that satisfies four criteria: (1) the elimination of neutral solute experiments for r_p and Δx_e characterization; (2) the removal of any explicit water flux expression from conventional DSPM-DE; (3) stronger guarantees of physically-representative membrane parameters; and (4) lower optimization residuals compared to sequential regression alternatives. To achieve these objectives, we propose a shift towards metaheuristic methods for global optimization in conjunction with maximum likelihood estimation (MLE).

2. Mathematical model

2.1. Transport in the selective layer

The extended Nernst-Planck equations combined with hindered transport relations are typically employed to characterize ion transport in the membrane's selective layer. Using this approach, the solute mole flux, J_j , can be expressed by the following differential equation:

$$J_j = -D_j K_{j,d} \frac{dC_j}{dx} + K_{j,c} C_j J_v - \frac{K_{j,d} D_j C_j z_j \mathfrak{F}}{RT} \frac{d\psi}{dx} \quad (1)$$

where $K_{j,d}$ and $K_{j,c}$ are the diffusive and convective hindrance factors, respectively (Deen, 1987; Ennis et al., 1996; Mavrouniotis and Brenner, 1988). In conventional DSPM-DE, relations for both hindrance factors depend on λ_j , the ratio of the solutes' Stokes radii to the membrane's pore radius (Labban et al., 2017). In Eq. (1), D_j is the solute diffusion coefficient in the bulk solution, z_j is its valence, and C_j is its concentration. Other variables and constants include: J_v , the water flux; ψ , the electric potential; T , the absolute temperature; \mathfrak{F} , Faraday's constant; and R , the universal gas constant. Here, x is the coordinate direction orthogonal to the membrane surface (as shown in Fig. 1). An electroneutrality constraint is needed to close the system of equations inside the membrane active layer:

$$\chi_d + \sum_{j=1}^{N_S} z_j C_j = 0 \quad (2)$$

where χ_d corresponds to the volumetric membrane charge density and N_S is the total number of ions in solution.

2.2. Concentration polarization

In DSPM-DE, ionic transport and concentration polarization in the fluid are accounted for by linearizing the extended Nernst-Planck equations in the feed stream, as shown by Gerales and Afonso (2007). Here, the solute flux in the feed-side boundary layer is given by the following relation:

$$J_j = -\bar{k}_{c,j} [C_{j,f,m} - C_{j,f,b}] + J_v C_{j,f,m} - z_j C_{j,f,m} D_j \frac{\mathfrak{F} \xi}{RT} \quad (3)$$

where ξ is the linearized electric potential gradient at the membrane-solution interface. Subscripts f and p denote the feed and permeate, respectively. Subscripts b and m denote the bulk and membrane interface, respectively. $\bar{k}_{c,j}$ is a modified mass transfer coefficient to account for the membrane permeation "suction effect" (Bird, 2002). $\bar{k}_{c,j}$ may be calculated as a function of $\omega_w \equiv J_v/k_{c,j}$, using Eq. (4):

$$\bar{k}_{c,j} = k_{c,j} [\omega_w + (1 + 0.26\omega_w^{1.4})]^{-1.7} \quad (4)$$

Here, $k_{c,j}$ is the conventional mass transfer coefficient, typically quantified by Sherwood mass transfer correlations. Depending on whether the membrane is employed in a hollow-fibre, spiral wound, or coupon-scale configuration, different correlations can be used (Labban et al., 2017).

Under steady-state operating conditions, the conservation of species can be used to express the solute flux as a function of the permeate concentration. This is combined with the extended Nernst-Planck equations in Eq. (3) to generate a full system of equations that are solved simultaneously (Oren et al., 2021). The last two conditions needed to close the system are the electroneutrality constraints on the feed and permeate sides (Rehman et al., 2021). These are formulated by Eqs. (5) and (6):

$$\sum_{j=1}^{N_S} z_j C_{j,f,m} = 0 \quad (5)$$

$$\sum_{j=1}^{N_S} z_j C_{j,p,b} = 0 \quad (6)$$

2.3. Solute partitioning

Although concentration may be discontinuous at the membrane interface, the chemical potential is continuous. This effect, commonly referred to as solute partitioning, can significantly impact ion selectivity (Lounder et al., 2022). The chemical potential is equal on both sides of the solution-membrane interface, $\mu_{0^-} = \mu_{0^+}$. In addition, both steric rejection and dielectric exclusion are incorporated using modifications posed by Giddings et al. (1968) and Gerales and Afonso (2007):

$$\frac{\gamma_j C_{j,f,m}|_{x=0^-}}{\gamma_j C_{j,f,m}|_{x=0^+}} = \phi_B \phi_S \exp \left(-\frac{z_j \mathfrak{F}}{RT} \Delta\psi_{D,f} \right) \quad (7)$$

Here, 0^- and 0^+ correspond to the fluid-side and membrane-side, respectively. $\Delta\psi_{D,f}$ is the Donnan potential that forms across the membrane at equilibrium on the feed-side and γ_j is the activity coefficient of species j . A corresponding expression is used for the permeate side. ϕ_S is an ion sieving coefficient, where $\phi_S \equiv (1 - \lambda_j)^2$. ϕ_B , the Born solvation coefficient, accounts for dielectric exclusion via ion solvation using the Born model (Dill and Bromberg, 2011). Here, ϕ_B is calculated using the Born solvation energy barrier:

$$\phi_B = \exp \left[-\frac{1}{kT} \frac{z_j^2 q^2}{8\pi\epsilon_0 r_j} \left(\frac{1}{\zeta_p} - \frac{1}{\zeta_b} \right) \right] \quad (8)$$

where q , ϵ_0 , and r_j are the fundamental electronic charge, permittivity of free space, and Stokes radius of species j , respectively. Finally, ζ_b corresponds to the dielectric constant in the fluid bulk.

In conventional DSPM-DE, the Davies model is commonly used to evaluate activity coefficients; however, the Davies model typically starts to diverge from experimental data for effective solute molalities above 0.8 mol/kg (Mistry et al., 2013). Pitzer–Kim’s multicomponent model shows stronger agreement with experiments, in some cases, all the way up to saturation (Pitzer, 1973). Consequently, we adopt the Pitzer–Kim model in this work. In the limit of dilute solutions, the Pitzer–Kim model converges to the Davies model (Mistry et al., 2013).

In solving the full DSPM-DE model, the presented equations are solved iteratively with three different residuals. Under-relaxation is also frequently required to avoid numerical instabilities that introduce oscillations and/or divergence (Chapra and Canale, 2001). Details of the numerical treatment are presented by Geraldes and Brites Alves (2008). In this work, the under-relaxation factor was varied to guarantee numerical convergence for all sets of experimental data tested for validation.

2.4. Proposed modifications

We now show how the membrane parameters can be obtained using only charged species experimental data. The traditional sequential regression procedure first quantifies r_p and Δx_e through two minimizations on uncharged rejection data (most often as a function of applied pressure), as seen in Eqs. (9) and (10). Using Eq. (9), first the difference between the model rejection, $\mathfrak{R}^{\text{mod}}$, and the experimental rejection, $\mathfrak{R}^{\text{exp}}$, is minimized to determine r_p . Once r_p is known, it is used as input into Eq. (10), which quantifies Δx_e using an explicit water flux relationship (some variations to this procedure exist, as detailed in Appendix A) that minimizes the difference between the model water flux, J_v^{mod} , and the experimental water flux, J_v^{exp} . Once both r_p and Δx_e have been quantified, they serve as inputs into a tertiary regression, presented in Eq. (11). Prior to this, zeta potential measurements are carried out to determine the isoelectric point (IEP) of the membranes, after which single-salt rejection experiments (most often using NaCl) are performed at the IEP to regress out ζ_p under the assumption that $\chi_d = 0$. Once ζ_p has been obtained, multi-component experiments can be performed using fixed values for r_p , Δx_e , and ζ_p to finally characterize χ_d using Eq. (12). The four objective functions are presented below (Ghorbani et al., 2021; Micari et al., 2020):

$$\argmin_{r_p} \sum_{i=1}^{N_v} \sum_{j=1}^{N_{\text{U}}} \left[\mathfrak{R}_{i,j}^{\text{mod}}(r_p) - \mathfrak{R}_{i,j}^{\text{exp}}(r_p) \right]^2 \quad (9)$$

$$\argmin_{\Delta x_e} \sum_{i=1}^{N_v} \left[J_{v,i}^{\text{mod}}(r_p, \Delta x_e) - J_{v,i}^{\text{exp}}(r_p, \Delta x_e) \right]^2 \quad (10)$$

$$\argmin_{\zeta_p} \sum_{i=1}^{N_v} \left[\mathfrak{R}_i^{\text{mod}}(r_p, \Delta x_e, \zeta_p, \chi_d = 0) - \mathfrak{R}_i^{\text{exp}}(r_p, \Delta x_e, \zeta_p, \chi_d = 0) \right]^2 \quad (11)$$

$$\argmin_{\chi_d} \sum_{i=1}^{N_v} \sum_{j=1}^{N_{\text{S}}} \left[\mathfrak{R}_{i,j}^{\text{mod}}(r_p, \Delta x_e, \zeta_p, \chi_d) - \mathfrak{R}_{i,j}^{\text{exp}}(r_p, \Delta x_e, \zeta_p, \chi_d) \right]^2 \quad (12)$$

In the above equations, iteration index i cycles through all water flux measurements, where N_v is the total number of water flux measurements taken for a given batch of experiments. N_v may take on different values for uncharged solute experiments, pure water permeability studies, single-salt experiments, and charged solute measurements. Iteration index j cycles through each solute (uncharged species in Eq. (9) and charged species in Eq. (12)). For uncharged solutes, the index cycles until N_{U} , while for charged species, the index cycles until N_{S} . In Eq. (9), the uncharged species rejection for a given solute j is calculated by solving the hindered convective-diffusive equation (derived in Appendix A):

$$\mathfrak{R}_j^{\text{mod}} = 1 - \frac{K_{j,c}(1 - \lambda_j)^2}{1 - [1 - K_{j,c}(1 - \lambda_j)^2] \exp(-\text{Pe}_j)} \quad (13)$$

where Pe_j is the Péclet number for species j .

In performing the minimizations, most studies in the literature adopt local optimization methods to determine membrane parameters (Kammoun et al., 2020; Labban et al., 2017; Micari et al., 2020). Common algorithms include the active-set method, trust region derivatives, Levenberg–Marquardt, Broyden–Fletcher–Goldfarb–Shanno (BFGS), among others (Chapra and Canale, 2001). In certain cases, not only is it possible to get stuck in local minima, but also to achieve optimization parameters that don’t align with physically-representative or experimentally-determined ranges (Kammoun et al., 2020).

To combat the mentioned shortcomings of traditional, local optimizations, we propose metaheuristic global optimization hybridized with gradient-free local search methods that *simultaneously* regress all four membrane parameters. In particular, we explore dual annealing; differential evolution; simplicial homology global optimization; and basin hopping - all algorithms available through Python’s SciPy library (Virtanen et al., 2020). The convergence criterion was kept constant across simulations with a tolerance of 10^{-6} . Our findings suggest that dual annealing (Kirkpatrick et al., 1983), in conjunction with the Nelder–Mead local optimizer (Nelder and Mead, 1965) provide the fastest convergence across investigated datasets.

The simultaneous regression requires a reformulation of the sequential minimization objective functions. This reformulation uses a multivariable regression supplemented with maximum likelihood estimators, $\sigma_{i,j}^2$, for each measurement to bias the regression towards more experimentally-confident values. $\sigma_{i,j}^2$ can be calculated using the conventional unbiased variance equation across multiple experimental trials. The resulting regression is:

$$\argmin_{r_p, \Delta x_e, \zeta_p, \chi_d} \sum_{i=1}^{N_v} \sum_{j=1}^{N_{\text{S}}} \frac{\left[\mathfrak{R}_{i,j}^{\text{mod}}(r_p, \Delta x_e, \zeta_p, \chi_d) - \mathfrak{R}_{i,j}^{\text{exp}}(r_p, \Delta x_e, \zeta_p, \chi_d) \right]^2}{\sigma_{i,j}^2} \quad (14)$$

Here, subscript i cycles through all charged species flux measurements and subscript j cycles through all charged species in solution.

The simultaneous regression by metaheuristic global optimization requires only data for charged species. Experimentalists can first directly measure flux and rejection (from permeance) using multiple charged species NF experiments and use these data as inputs for $\mathfrak{R}_{i,j}^{\text{exp}}$ and $\sigma_{i,j}^2$ across multiple trials for characterization.

3. Results and discussion

The proposed regression framework is tested against eight different datasets comprising of both commercially-available and lab-fabricated membranes at different input salinities and compositions. The total number of ions in solution across all eight datasets did not exceed six¹, and the average number of flux measurements per ion was between five and

¹ Using more than six solutes can often lead to significant solute-solute coupling, which the extended Nernst–Planck equations intrinsically neglect.

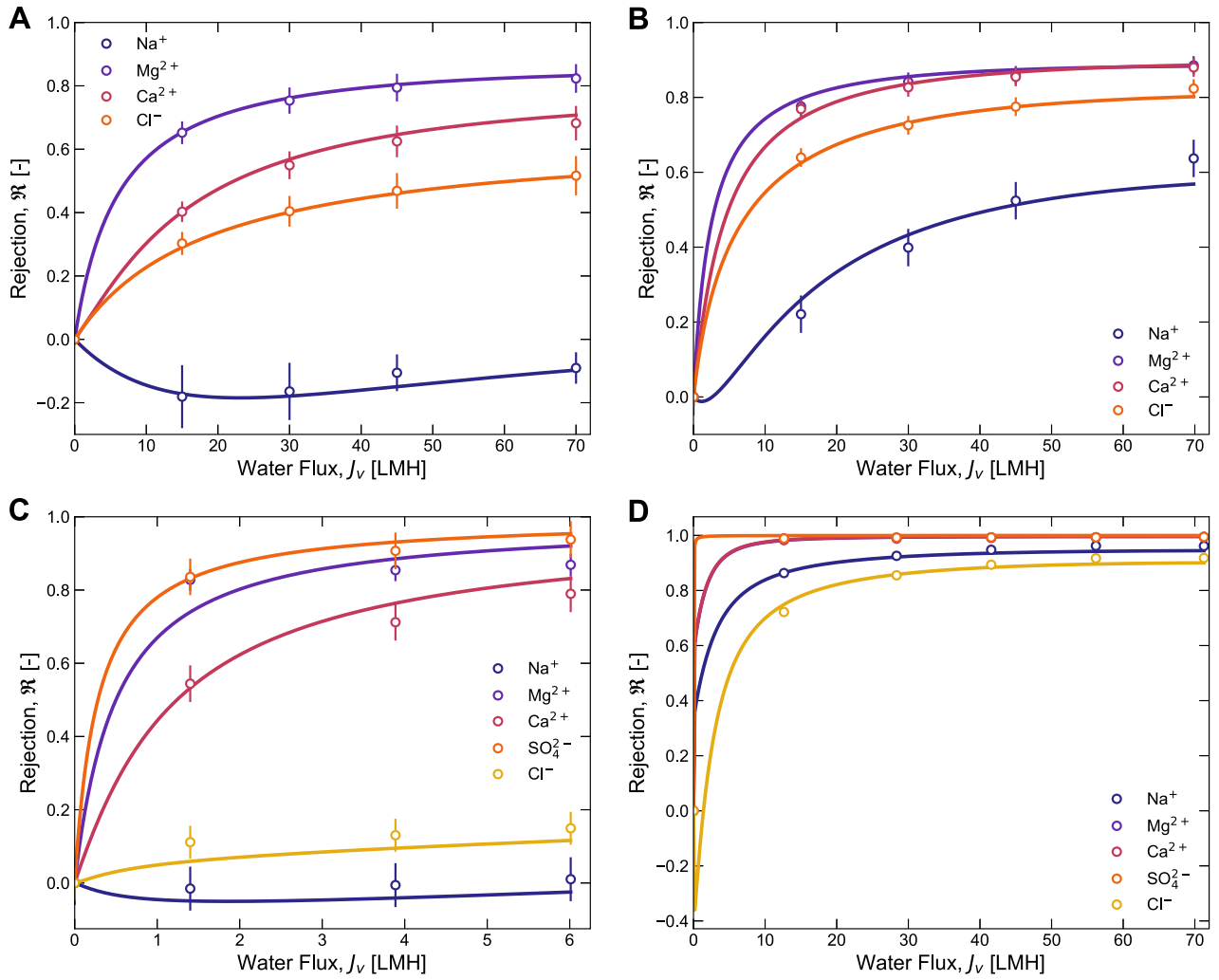


Fig. 2. Rejection regression against water flux across four sample datasets. (A) and (B) correspond to experimental data obtained from the study by Micari et al. (Micari et al., 2020). Here, there are only four ions present in the solution, and a percentage deviation of 4% and 9% is achieved for NF270 and TS80, respectively, compared to the 15% achieved in the original work (Micari et al., 2020). (C) is data from Labban et al.'s LbL1.5-C membrane and (D) corresponds to Kammoun et al.'s studies on NF90 (Kammoun et al., 2020; Labban et al., 2017). Both of these studies have five ions in solution, and required over nine times more time to regress compared to Micari et al.'s data. The deviation achieved from our regression was 9% and 4%, compared to the 12% and 7% values, obtained by Labban et al. and Kammoun et al., respectively.

eight. The results obtained by previous studies were initially validated using their proposed parameters from DSPM-DE (Kammoun et al. used NanoFlux™ to perform their minimization), before the modified regression framework was tested. Rejection as a function of water flux is presented in Fig. 2 for four sample analyses.

In Fig. 2, strong agreement between our proposed regression approach and the experimental data can be observed. For NF270 and TS80 membranes, Micari et al. reported mean absolute deviations of DSPM-DE from their data of around 15% across all conducted regressions (Micari et al., 2020). Here, for NF270 and TS80 membranes, the new regression methodology achieves a mean absolute deviation of 2% and 9%, respectively. In addition, Micari et al. used the Hagen-Poiseuille expression to quantify r_p and Δx_e ; however, substantially different pore radii were obtained across their neutral solute experiments, leading to an average value being used for χ_d and ζ_p characterization. In our approach, the need for an explicit water flux expression is eliminated, and the resulting values of r_p and Δx_e are similar to those reported by Micari et al. and to those available in the literature for both sets of membranes (Dang et al., 2014; Micari et al., 2020). Simultaneously, lower residuals are achieved, even with fewer experimental data serving as model inputs.

Labban et al. and Kammoun et al. obtained mean absolute deviations of 12% and 7% for LbL1.5-C and NF90 membranes, respectively (Kammoun et al., 2020; Labban et al., 2017). Using our approach, we are able to achieve 9% and 4% deviations for Labban et al. and Kammoun et al.'s data, respectively. Similarly to Micari et al.'s studies, Labban et al. use the Hagen-Poiseuille equation to evaluate r_p and Δx_e ; again, our modified regression framework achieves lower residuals, with no water flux expression, and reduced data requirements. These results illustrate our approach's ability to obtain higher accuracy solutions with smaller datasets. Four more analyses are performed on experimental data for NF270, CD-NF-50, PSS/PAH_{2.5}, and PSS/PAH_{2.5}-X membranes (Bandini and Vezzani, 2003; Dong et al., 2022; Vezzani and Bandini, 2002); our optimal parameters and those from the literature are plotted for comparison in Fig. 3 (for cases where past studies reported values).

In the analyses, we also noted results obtained by previous studies that appear to deviate from physically-representative values. For example, at a certain salinity and composition, Kammoun et al. reported a value of $\Delta x_e = 8.92 \mu\text{m}$ for NF90 membranes (other values obtained went up to $\Delta x_e = 35 \mu\text{m}$). Experiments from the literature have noted effective thicknesses between 0.8 and 2 μm (Mohammad et al., 2007; Richards et al., 2013; Thabo et al., 2021), indicating the divergence

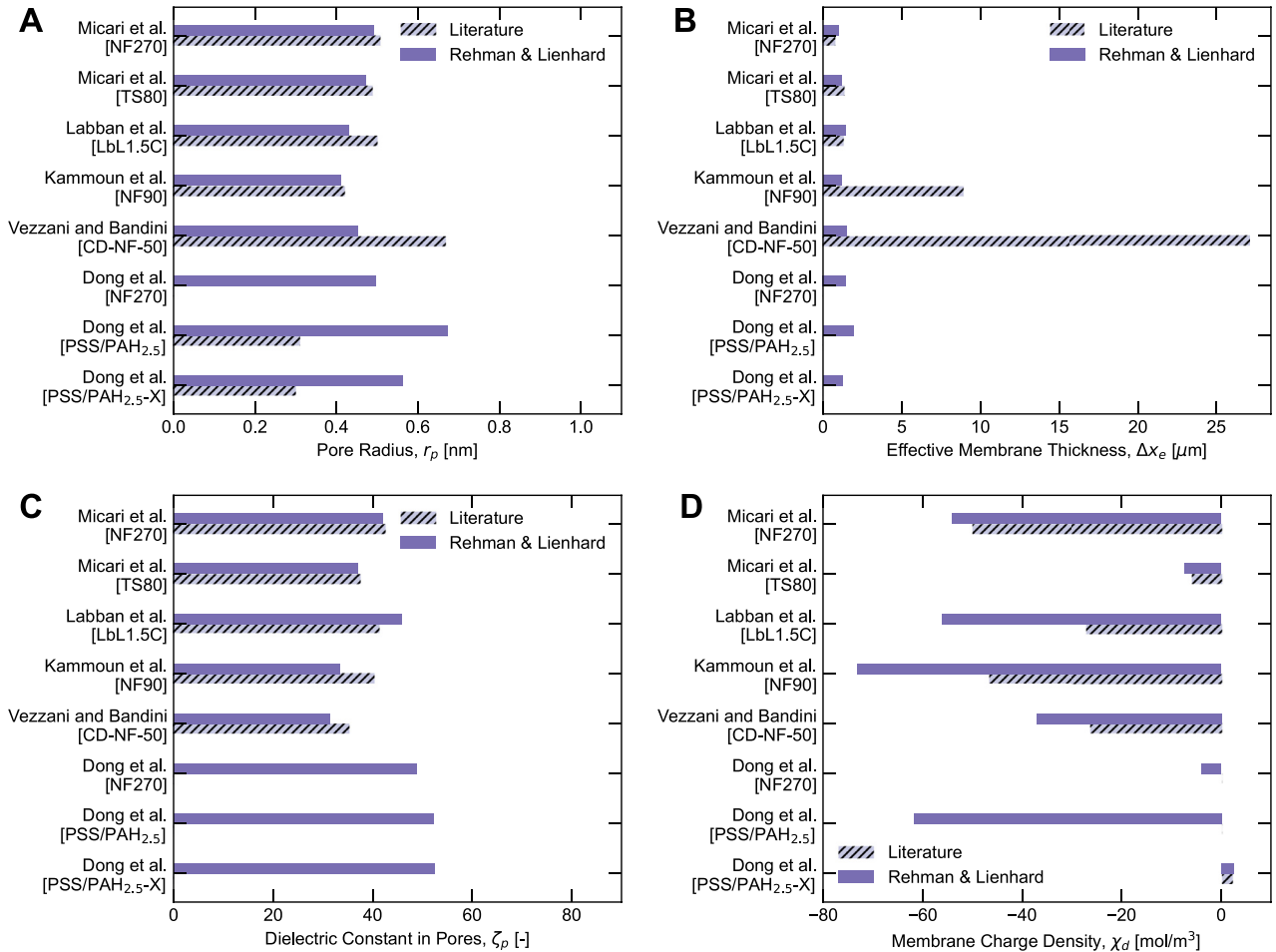


Fig. 3. Regressed parameters compared to those obtained from literature. Values are relatively similar across all experimental datasets. For all the regressed parameters, the absolute percentage deviations obtained were lower than those obtained across the literature when DSPM-DE was used. *Note:* Dong et al. did not provide data for effective membrane thickness and the dielectric constant. The values of membrane charge density are 2.10 mol/m³ and 2.45 mol/m³ by Dong et al. and our regression, respectively, since they appear too small to discern from the figure.

of the DSPM-DE model from representative values when the conventional methodology is applied. In our approach, the global optimization and MLE enable reduced residuals with a substantially more accurate $\Delta x_e = 1.16 \mu\text{m}$. This value is the global minimum and is more consistent with experiments from literature. These findings underscore the value of global optimization methods in characterizing NF membranes.

Across all studies conducted, lower optimization residuals were noted. These findings suggest that with only charged species data, we can still accurately infer the values of the conventional membrane characterization parameters. Our results also support the elimination of explicit water flux relationships to characterize pore radii and effective membrane thicknesses across a range of diverse salinities, compositions, and membranes.

4. Summary

In this work, we present a new regression methodology for characterizing NF membranes. The framework harnesses metaheuristic methods for combined global-local optimization and combines them with maximum likelihood estimation. Our results illustrate an approach that can substantially improve optimization residuals, eliminate the need for neutral solute experiments, remove the dependence on any explicit water flux equations, and provide stricter guarantees of more experimentally-aligned regression parameters. The framework was validated against eight independent sets of data across various input salinities, compositions, and membranes. In all studied cases, the proposed

methodology showed improved performance compared to sequential regression alternatives.

Declaration of Competing Interest

The authors declare that they have no known competing financial interests or personal relationships that could have appeared to influence the work reported in this paper.

Acknowledgements

The authors would like to thank the Centers for Mechanical Engineering Research and Education at MIT and SUSTech (MechERE Centers at MIT and SUSTech) for partially funding the research reported here. Danyal would also like to acknowledge financial support provided by a fellowship from the Abdul Latif Jameel World Water and Food Systems (J-WAFS) Lab and fellowship support from the Martin Family Society of Fellows.

Appendix A. Regression of uncharged solutes

This appendix briefly summarizes the treatment of uncharged solutes in the literature. The restricted flux in the selective layer of solute j when convection and diffusion govern transport can be written as follows:

$$J_j = -H_{j,d} D_j \frac{dc_j}{dx} + H_{j,c} J_v c_j \quad (\text{A.1})$$

where $H_{j,d}$ and $H_{j,c}$ are modified convective and diffusive hindrance factors with integrated partition coefficients. By integrating both sides of the equation, we obtain the following:

$$\int_{c_{j,f}}^{c_{j,p}} \frac{1}{H_{j,c} J_v c_j - J_j} dc_j = \int_0^{\Delta x_e} \frac{1}{H_{j,d} D_j} dx \quad (\text{A.2})$$

Here, we integrate from the feed side to the permeate side, under the assumption that the concentrations are low enough for insignificant boundary layer formation - this condition is met by running experiments with high cross-flow velocities to prevent concentration polarization (Bowen et al., 1997; Schaep et al., 1999). Integrating the result yields the following expression:

$$\ln \left(\frac{H_{j,c} J_v c_{j,p} - J_j}{H_{j,c} J_v c_{j,f} - J_j} \right) = \frac{H_{j,c} J_v \Delta x_e}{H_{j,d} D_j} \quad (\text{A.3})$$

where the right-hand-side of the equation corresponds to the ratio of convective transport to diffusive transport, often termed the Péclet number:

$$\text{Pe}_j \equiv \frac{H_{j,c} J_v \Delta x_e}{H_{j,d} D_j} \quad (\text{A.4})$$

Upon exponentiating both sides of Eq. (A.3) and setting $J_v c_{j,p} = J_j$ (an approximation of purely convective transport in the permeate stream), the following expression is found:

$$\frac{J_j(1 - H_{j,c})}{J_j - H_{j,c} J_v c_{j,f}} = \exp(\text{Pe}_j) \quad (\text{A.5})$$

Rearranging for J_j , we obtain:

$$J_j = \frac{H_{j,c} J_v c_{j,f}}{1 - (1 - H_{j,c}) \exp(-\text{Pe}_j)} \quad (\text{A.6})$$

As $H_{j,c} \equiv K_{j,c}(1 - \lambda_j)^2$ and $H_{j,d} \equiv K_{j,d}(1 - \lambda_j)^2$ (modifications that account for steric exclusion), we can re-write Eq. (A.6) as:

$$J_j = \frac{K_{j,c}(1 - \lambda_j)^2 J_v c_{j,f}}{1 - [1 - K_{j,c}(1 - \lambda_j)^2] \exp(-\text{Pe}_j)} \quad (\text{A.7})$$

Finally, we divide both sides by $J_v c_{j,f}$, replace J_j with $J_v c_{j,p}$, and subtract the equation from 1 to obtain uncharged solute rejection, $\mathfrak{R}_j^{\text{mod}}$:

$$\mathfrak{R}_j^{\text{mod}} \equiv 1 - \frac{c_{j,p}}{c_{j,f}} = 1 - \frac{K_{j,c}(1 - \lambda_j)^2}{1 - [1 - K_{j,c}(1 - \lambda_j)^2] \exp(-\text{Pe}_j)} \quad (\text{A.8})$$

This equation characterizes the rejection of uncharged solutes when no boundary layers are present in the feed or permeate streams. By substituting the Hagen-Poiseuille equation into Pe_j , the rejection becomes a function of only the pore radius, and removes the dependence on the membrane thickness i.e. $\mathfrak{R}_j^{\text{mod}}(r_p, \Delta x_e) \rightarrow \mathfrak{R}_j^{\text{mod}}(r_p)$:

$$\text{Pe}_j(r_p, \Delta x_e) = \frac{H_{j,c} \Delta x_e}{H_{j,d} D_j} \cdot \underbrace{\frac{r_p^2 \Delta P}{8 \mu \Delta x_e}}_{J_v} = \frac{H_{j,c} r_p^2 \Delta P}{8 \mu H_{j,d} D_j} = \text{Pe}_j(r_p) \quad (\text{A.9})$$

where μ is the dynamic viscosity and the Hagen-Poiseuille equation is substituted in for J_v . The Hagen-Poiseuille equation claims fully developed laminar flow in a straight circular tube as a model for membrane pore networks, which may not represent the physics of the problem being modeled. This substitution also introduces the applied pressure, ΔP , an easy-to-measure independent parameter. Some authors also replace ΔP with ΔP_{eff} , which purports to account for the osmotic pressure difference between the feed and permeate streams (Bandini and Vezzani, 2003; Wang and Lin, 2021).

In certain cases, instead of using $\mathfrak{R}_j^{\text{mod}}$ in the first regression, Eq. (9), some authors replace it with the rejection in the high Péclet number regime, $\mathfrak{R}_j^{\text{lim}}$. When $\text{Pe}_j \rightarrow \infty$, $\mathfrak{R}_j^{\text{mod}} \rightarrow \mathfrak{R}_j^{\text{lim}}$, where $\mathfrak{R}_j^{\text{lim}} = 1 - K_{j,c}(1 - \lambda_j)^2$ (Labban et al., 2017). This value is often termed the limiting rejection.

Once the pore radius is regressed from uncharged solute rejection data, its value is put back into the Hagen-Poiseuille equation, which is then used to regress out membrane thickness by fitting the water flux to applied pressure data via Eq. (10) (Micari et al., 2020).

Slight variations of this approach also exist in the literature. In some cases, instead of using Eqs. (9) and (10) from the main text, authors combine the minimization into a simultaneous regression for water flux and uncharged species rejection (Wang et al., 2021). This leads to the following objective function:

$$\begin{aligned} \text{argmin}_{r_p, \Delta x_e} \sum_{i=1}^{N_v} \left[\frac{J_{v,i}^{\text{mod}}(r_p, \Delta x_e) - J_{v,i}^{\text{exp}}(r_p, \Delta x_e)}{J_{v,i}^{\text{exp}}(r_p, \Delta x_e)} \right]^2 \\ + \sum_{i=1}^{N_v} \sum_{j=1}^{N_{ij}} \left[\frac{\mathfrak{R}_{i,j}^{\text{mod}}(r_p, \Delta x_e) - \mathfrak{R}_{i,j}^{\text{exp}}(r_p, \Delta x_e)}{\mathfrak{R}_{i,j}^{\text{exp}}(r_p, \Delta x_e)} \right]^2 \end{aligned} \quad (\text{A.10})$$

This formulation employs a simultaneous regression for water flux and rejection, but still requires an explicit water flux equation. These approaches cover the most frequently used methodologies for performing NF membrane characterization in the literature.

References

- Bandini, S., Vezzani, D., 2003. Nanofiltration modeling: the role of dielectric exclusion in membrane characterization. *Chem. Eng. Sci.* 58 (15), 3303–3326. doi:10.1016/S0009-2509(03)00212-4.
- Bird, R.B., 2002. Transport phenomena. *Appl. Mech. Rev.* 55 (1), R1–R4. doi:10.1115/1.1424298. https://asmedigitalcollection.asme.org/appliedmechanicsreviews/article-pdf/55/1/R1/5438575/r1_1.pdf
- Bowen, R.W., Mohammad, W.A., Hilal, N., 1997. Characterisation of nanofiltration membranes for predictive purposes use of salts, uncharged solutes and atomic force microscopy. *J. Membr. Sci.* 126 (1), 91–105. doi:10.1016/S0376-7388(96)00276-1.
- Chapra, S.C., Canale, R., 2001. *Numerical Methods for Engineers: With Software and Programming Applications*, fourth ed. McGraw-Hill Higher Education.
- Cheng, W., Liu, C., Tong, T., Epsztein, R., Sun, M., Verduzco, R., Ma, J., Elimelech, M., 2018. Selective removal of divalent cations by polyelectrolyte multilayer nanofiltration membrane: role of polyelectrolyte charge, ion size, and ionic strength. *J. Membr. Sci.* 559, 98–106. doi:10.1016/j.memsci.2018.04.052.
- Dang, H.Q., Price, W.E., Nghiem, L.D., 2014. The effects of feed solution temperature on pore size and trace organic contaminant rejection by the nanofiltration membrane NF270. *Sep. Purif. Technol.* 125, 43–51. doi:10.1016/j.seppur.2013.12.043.
- Deen, W.M., 1987. Hindered transport of large molecules in liquid-filled pores. *AIChE J.* 33 (9), 1409–1425. doi:10.1002/aic.690330902. <https://aiche.onlinelibrary.wiley.com/doi/pdf/10.1002/aic.690330902>
- Dill, K.A., Bromberg, S., 2011. *Molecular Driving Forces: Statistical Thermodynamics in Biology, Chemistry, Physics, and Nanoscience*. Garland Science.
- Dong, C., He, R., Xu, S., He, H., Chen, H., Zhang, Y.-B., He, T., 2022. Layer-by-layer (LbL) hollow fiber nanofiltration membranes for seawater treatment: ion rejection. *Desalination* 534, 115793. doi:10.1016/j.desal.2021.115793.
- Ennis, J., Zhang, H., Stevens, G.W., Perera, J.M., Scales, P.J., Carnie, S.L., 1996. Mobility of protein through a porous membrane. *J. Membr. Sci.* 119 (1), 47–58. doi:10.1016/0376-7388(96)00112-3.
- Geraldes, V., Afonso, M.D., 2007. Prediction of the concentration polarization in the nanofiltration/reverse osmosis of dilute multi-ionic solutions. *J. Membr. Sci.* 300 (1), 20–27. doi:10.1016/j.memsci.2007.04.025.
- Geraldes, V., Brites Alves, A.M., 2008. Computer program for simulation of mass transport in nanofiltration membranes. *J. Membr. Sci.* 321 (2), 172–182. doi:10.1016/j.memsci.2008.04.054.
- Ghorbani, A., Bayati, B., Drioli, E., Macedonio, F., Kikavani, T., Frappa, M., 2021. Modeling of nanofiltration process using DSPM-DEmodel for purification of amine solution. *Membranes* 11 (4), 230. doi:10.3390/membranes11040230.
- Giddings, J.C., Kucera, E., Russell, C.P., Myers, M.N., 1968. Statistical theory for the equilibrium distribution of rigid molecules in inert porous networks. exclusion chromatography. *J. Phys. Chem.* 72 (13), 4397–4408. doi:10.1021/j100859a008.
- Hardian, R., Cwyar, R.M., Chen, E.Y.-X., Szekely, G., 2022. Sustainable nanofiltration membranes based on biosourced fully recyclable polyesters and green solvents. *J. Membrane Sci. Lett.* 2 (1), 100016. doi:10.1016/j.memlet.2022.100016.
- Kammoun, M.A., Gassara, S., Palmeri, J., Amar, B., Deratani, A., 2020. Nanofiltration performance prediction for brackish water desalination: case study of Tunisian groundwater. *Desalination Water Treat.* 181, 27–39. doi:10.5004/dwt.2020.25100.
- Kirkpatrick, S., Gelatt, D.C., Vecchi, M.P., 1983. Optimization by simulated annealing. *Science* 220 (4598), 671–680. doi:10.1126/science.220.4598.671.
- Labban, O., Liu, C., Chong, T.H., Lienhard, J.H., 2017. Fundamentals of low-pressure nanofiltration: membrane characterization, modeling, and understanding the multi-ionic interactions in water softening. *J. Membr. Sci.* 521, 18–32. doi:10.1016/j.memsci.2016.08.062.
- Louder, S.J., Wright, P.T., Mazzaferro, L., Asatekin, A., 2022. Fouling-resistant membranes with tunable pore size fabricated using cross-linkable copolymers with high zwitterion content. *J. Membr. Sci. Lett.* 2 (1), 100019. doi:10.1016/j.memlet.2022.100019.

- Mavrovouniotis, G.M., Brenner, H., 1988. Hindered sedimentation, diffusion, and dispersion coefficients for brownian spheres in circular cylindrical pores. *J. Colloid Interface Sci.* 124 (1), 269–283. doi:[10.1016/0021-9797\(88\)90348-7](https://doi.org/10.1016/0021-9797(88)90348-7).
- Micari, M., Diamantidou, D., Heijman, S.G., Moser, M., Haidari, A., Spanjers, H., Bertsch, V., 2020. Experimental and theoretical characterization of commercial nanofiltration membranes for the treatment of ion exchange spent regenerant. *J. Membr. Sci.* 606, 118117. doi:[10.1016/j.memsci.2020.118117](https://doi.org/10.1016/j.memsci.2020.118117).
- Mistry, K.H., Hunter, H.A., Lienhard, J.H., 2013. Effect of composition and nonideal solution behavior on desalination calculations for mixed electrolyte solutions with comparison to seawater. *Desalination* 318, 34–47. doi:[10.1016/j.desal.2013.03.015](https://doi.org/10.1016/j.desal.2013.03.015).
- Mohammad, W.A., Hilal, N., Al-Zoubi, H., Darwish, N.A., 2007. Prediction of permeate fluxes and rejections of highly concentrated salts in nanofiltration membranes. *J. Membr. Sci.* 289 (1), 40–50. doi:[10.1016/j.memsci.2006.11.035](https://doi.org/10.1016/j.memsci.2006.11.035).
- Nelder, J.A., Mead, R., 1965. A simplex method for function minimization. *Comput. J.* 7 (4), 308–313. doi:[10.1093/comjnl/7.4.308](https://doi.org/10.1093/comjnl/7.4.308).
- Oren, Y.S., Freger, V., Nir, O., 2021. New compact expressions for concentration-polarization of trace-ions in pressure-driven membrane processes. *J. Membr. Sci. Lett.* 1 (1), 100003. doi:[10.1016/j.memlet.2021.100003](https://doi.org/10.1016/j.memlet.2021.100003).
- Pitzer, K.S., 1973. Thermodynamics of electrolytes. I. Theoretical basis and general equations. *J. Phys. Chem.* 77 (2), 268–277. doi:[10.1021/j100621a026](https://doi.org/10.1021/j100621a026).
- Puhan, M.R., Sutariya, B., Karan, S., 2022. Revisiting the alkali hydrolysis of polyamide nanofiltration membranes. *J. Membr. Sci.* 661, 120887. doi:[10.1016/j.memsci.2022.120887](https://doi.org/10.1016/j.memsci.2022.120887).
- Rehman, D., Ahdab, Y.D., Lienhard, J.H., 2021. Monovalent selective electrodialysis: modelling multi-ionic transport across selective membranes. *Water Res.* 199, 117171. doi:[10.1016/j.watres.2021.117171](https://doi.org/10.1016/j.watres.2021.117171).
- Richards, L.A., Richards, B.S., Corry, B., Schfer, A.I., 2013. Experimental energy barriers to anions transporting through nanofiltration membranes. *Environ. Sci. Technol.* 47 (4), 1968–1976. doi:[10.1021/es303925r](https://doi.org/10.1021/es303925r).
- Ritt, C.L., Liu, M., Pham, T.A., Epsztein, R., Kulik, H.J., Elimelech, M., 2022. Machine learning reveals key ion selectivity mechanisms in polymeric membranes with sub-nanometer pores. *Sci. Adv.* 8 (2), EABL5771. doi:[10.1126/sciadv.abl5771](https://doi.org/10.1126/sciadv.abl5771).
- Roy, Y., Sharqawy, M.H., Lienhard, J.H., 2015. Modeling of flat-sheet and spiral-wound nanofiltration configurations and its application in seawater nanofiltration. *J. Membr. Sci.* 493, 360–372. doi:[10.1016/j.memsci.2015.06.030](https://doi.org/10.1016/j.memsci.2015.06.030).
- Schaep, J., Vandecasteele, C., Mohammad, W.A., Bowen, R.W., 1999. Analysis of the salt retention of nanofiltration membranes using the donnan steric partitioning pore model. *Sep. Sci. Technol.* 34 (15), 3009–3030. doi:[10.1081/SS-100100819](https://doi.org/10.1081/SS-100100819).
- Shinde, D.B., Cao, L., Liu, X., Wonanke, D.A., Zhou, Z., Hedhili, M.N., Addicoat, M., Huang, K.-W., Lai, Z., 2021. Tailored pore size and microporosity of covalent organic framework (COF) membranes for improved molecular separation. *J. Membr. Sci. Lett.* 1 (2), 100008. doi:[10.1016/j.memlet.2021.100008](https://doi.org/10.1016/j.memlet.2021.100008).
- Sholl, D.S., Lively, R.P., 2016. Seven chemical separations to change the world. *Nature* 532 (7600), 435–437. doi:[10.1038/532435a](https://doi.org/10.1038/532435a).
- Silva, P., Han, S., Livingston, A.G., 2005. Solvent transport in organic solvent nanofiltration membranes. *J. Membr. Sci.* 262 (1), 49–59. doi:[10.1016/j.memsci.2005.03.052](https://doi.org/10.1016/j.memsci.2005.03.052).
- Thabo, B., Okoli, B.J., Modise, S.J., Nelana, S., 2021. Rejection capacity of nanofiltration membranes for nickel, copper, silver and palladium at various oxidation states. *Membranes* 11 (9), 653. doi:[10.3390/membranes11090653](https://doi.org/10.3390/membranes11090653).
- Vezzani, D., Bandini, S., 2002. Donnan equilibrium and dielectric exclusion for characterization of nanofiltration membranes. *Desalination* 149 (1), 477–483. doi:[10.1016/S0011-9164\(02\)00784-1](https://doi.org/10.1016/S0011-9164(02)00784-1).
- Virtanen, P., Gommers, R., Oliphant, T.E., Haberland, M., Reddy, T., Cournapeau, D., Burovski, E., Peterson, P., Weckesser, W., Bright, J., van der Walt, S.J., Brett, M., Wilson, J., Millman, K.J., Mayorov, N., Nelson, A.R.J., Jones, E., Kern, R., Larson, E., Carey, C.J., Polat, İ., Feng, Y., Moore, E.W., VanderPlas, J., Laxalde, D., Perktold, J., Cimrman, R., Henriksen, I., Quintero, E.A., Harris, C.R., Archibald, A.M., Ribeiro, A.H., Pedregosa, F., van Mulbregt, P., SciPy 1.0 Contributors, 2020. SciPy 1.0: fundamental algorithms for scientific computing in Python. *Nat. Methods* 17, 261–272. doi:[10.1038/s41592-019-0686-2](https://doi.org/10.1038/s41592-019-0686-2).
- Wang, L., Rehman, D., Sun, P.-F., Deshmukh, A., Zhang, L., Han, Q., Yang, Z., Wang, Z., Park, H.-D., Lienhard, J.H., Tang, C.Y., 2021. Novel positively charged metal-coordinated nanofiltration membrane for lithium recovery. *ACS Appl. Mater. Interfaces* 13 (14), 16906–16915. doi:[10.1021/acsami.1c02252](https://doi.org/10.1021/acsami.1c02252).
- Wang, R., Lin, S., 2021. Pore model for nanofiltration: history, theoretical framework, key predictions, limitations, and prospects. *J. Membr. Sci.* 620, 118809. doi:[10.1016/j.memsci.2020.118809](https://doi.org/10.1016/j.memsci.2020.118809).
- Zydney, A.L., 2022. Development of a new blocking model for membrane fouling based on a composite media model. *J. Membr. Sci. Lett.* 2 (1), 100018. doi:[10.1016/j.memlet.2022.100018](https://doi.org/10.1016/j.memlet.2022.100018).